

Design and performance analysis of a 3-RRR spherical parallel manipulator for hip exoskeleton applications

Soheil Sadeqi, Shaun P Bourgeois, Edward J Park and Siamak Arzanpour

Abstract

This paper presents the design and performance analysis and experimental study of a 3-RRR spherical parallel manipulator in the context of hip exoskeleton applications. First, the mechanism's inverse kinematics analysis and Jacobian matrix development are revisited. Manipulability, dexterity, and rotational sensitivity indices are then evaluated for two different methods of attachment to the human body. The superior attachment method in terms of these performance measures is indicated, and an experimental study based on the selected method is conducted; the experiment involves testing the capability of a 3-RRR manipulator's end-effector in tracking the motions experienced by a human hip joint during normal gait cycles. Finally, the results of the experimental study indicate that the manipulator represents a feasible hip exoskeleton solution providing total kinematic compliance with the human hip joint's 3-degree-of-freedom motion capabilities.

Keywords

Hip exoskeleton, spherical parallel manipulator, inverse kinematics, Jacobian, dexterity, manipulability, rotational sensitivity, experimental data

Date received: 27 October 2016; accepted: 30 January 2017

Introduction

An exoskeleton is a wearable robot designed to supplement one or more abilities of the human body part to which it is connected. Exoskeleton usage is often motivated by energy conservation for functional bodily limbs or strength assistance for limbs that have weakened or total loss of functionality. These capabilities stand to improve the quality of life for people suffering from mobility disablements, which have been reported to affect approximately 20,639,200 non-institutionalized individuals in the United States (7.1% of the total US population) in 2013¹ and 2,512,800 Canadians (7.2% of the total Canadian population) in 2012.²

The presence of one or more joints with multiple active degrees-of-freedom (DOFs) in the pertinent limb complicates the design of an exoskeleton with complete kinematic compliance. One method to address this challenge is to restrict the motions that the exoskeleton supports about the multi-DOF joint, instead of providing total kinematic compliance.

This is the common design method for current exoskeleton research and technologies.^{3–6} Consequently, most present-day exoskeletons are composed of kinematic open chains: serially connected single-DOF rotary or prismatic joints between rigid linkages. However, Kizir and Bingul conclude that closed-chain parallel manipulators (PMs) have better performance than their serial manipulator counterparts with regard to positioning accuracy, speed, force application, and payload-to-weight ratio.⁷ Thus, in order to improve the robotic performance and kinematic functionality of exoskeletons, we propose the use of parallel robots paired with a mechanical structure that transmits motions to the targeted body part in a comfortable,

School of Mechatronic Systems Engineering, Simon Fraser University, Surrey, British Columbia, Canada

Corresponding author:

Siamak Arzanpour, Simon Fraser University, 250-13450 102 Ave, Surrey, British Columbia V3T 0A3, Canada.
Email: arzanpour@sfu.ca



non-restrictive way. One parallel robotic structure that has potential for use in such an application is the 3-RRR spherical parallel manipulator. Among previous works in the literature, Gosselin and Angeles present an inverse kinematics analysis, along with discussions of design optimization and singularities, for this manipulator.⁸ Gosselin and Lavoie further discuss the kinematic design and Jacobian derivation for the mechanism.⁹ Gosselin and Hamel have gone on to present a specific embodiment of the manipulator, the Agile Eye;¹⁰ Gosselin and St-Pierre have further developed its kinematic description and experimentation.¹¹ More recently, Bai *et al.* have revisited the forward displacement analysis of the 3-RRR manipulator and introduced a new embodiment, called the Agile Wrist.¹² Wang *et al.* have conceptualized, analyzed (i.e. kinematic performance), and completed experiments (i.e. torque study) on the use of a redundantly actuated 3-RUS/RRR manipulator for 3-DOF ankle rehabilitation.¹³ Most recently, Niyetkalyev and Shintemirov detail one method of obtaining forward and inverse kinematics solutions for the Agile Wrist design, including simulation results and numerical examples for verification.¹⁴

This paper investigates the performance of the 3-RRR in the context of exoskeleton applications. Specifically, manipulability, dexterity, and rotational sensitivity performance indices are evaluated for two different body-interfacing schemes of the manipulator when it is applied as a hip exoskeleton device; here it is assumed that the manipulator supports 3-DOF rotational motions of the upper leg with respect to the pelvis. Our findings suggest that a 3-RRR manipulator can be employed as the hip actuator in an exoskeleton system; this represents an original contribution to the field of exoskeleton research.

Kinematic considerations for the 3-RRR manipulator

Kinematic architecture

Figure 1 shows a geometrical schematic of a generalized 3-RRR manipulator. This device is considered a 3-DOF spherical mechanism because all of its moving linkages perform spherical motions about a common point, O , which is stationary with respect to its base structure.^{15,16} That is, all particles' motions within the system can be unambiguously described by radial projections on the surface of a unit sphere centered at the aforementioned stationary point. Consequently, the only permissible lower-pair joint within a spherical mechanism's limbs is a revolute joint; furthermore, all joint axes must intersect at the common stationary point mentioned above. In Figure 1, linkages are

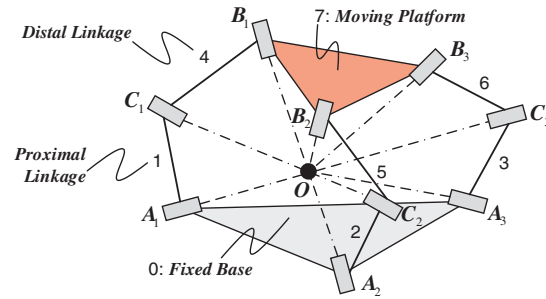


Figure 1. Schematic illustration of a generalized 3-RRR manipulator.¹⁶

labeled 0–7, where 0 indicates the fixed base structure and 7 corresponds to the manipulator's end-effector (i.e. the moving platform). A_i , B_i , and C_i denote the three revolute joints of each limb i , where $i = 1, 2, 3$ and only A_i joints are active.

Note that two notable embodiments of the 3-RRR manipulator are the Agile Eye and Agile Wrist, as mentioned in the previous section and shown in Figure 2(a) and (b), respectively. Although mechanically distinct, these two embodiments have the same inverse kinematics procedure, which is reviewed in the subsection that follows.

Inverse kinematics derivation

Inverse kinematics analysis for the 3-RRR manipulator has been examined extensively.^{8,9,11,12} One approach is briefly revisited here for the sake of completeness and to acclimatize the reader to the notations and naming conventions used subsequently in this paper.

To start, direction vectors \mathbf{u}_1 , \mathbf{u}_2 , and \mathbf{u}_3 specify the rotational axes of the system's three active A_i joints, as shown in Figure 3. These vectors have constant values with respect to the global frame (with origin O) because they correspond to fixed joints. Next, input scalar variables θ_1 , θ_2 , and θ_3 define the angular states of the respective active joints. Direction vectors \mathbf{w}_1 , \mathbf{w}_2 , and \mathbf{w}_3 in turn specify the rotational axes of the joints between the three proximal–distal link pairs (i.e. the C_i joints). These vectors vary in element values with respect to the global frame because they correspond to free joints. The final set of direction vectors, \mathbf{v}_1 , \mathbf{v}_2 , and \mathbf{v}_3 , specify the rotational axes of the joints between the three connection points of the distal links to the end effector (i.e. the B_i joints). Again, these vectors vary with respect to the global frame because they correspond to free joints.

Scalar constant α_1 specifies the angle between each actuated A_i joint and the corresponding proximal C_i joint within the plane containing both of these joints as well as the global origin, O . The value of α_1 used for the 3-RRR design analyzed here is 90° . The second

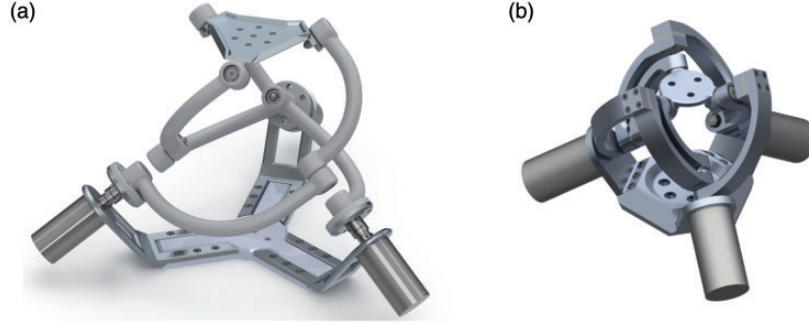


Figure 2. (a) Agile Eye and (b) Agile Wrist embodiments of the 3-RRR manipulator.

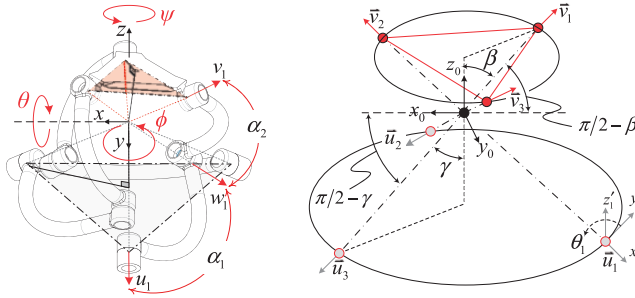


Figure 3. 3-RRR schematics with parameters and direction vectors labelled.

scalar constant, α_2 , specifies the angle between each proximal C_i joint and the corresponding distal B_i joint within the plane containing both of these joints as well as the global origin. The value of α_2 used for the 3-RRR design considered here is also 90° . Third, scalar constant β indicates the angle between the \mathbf{v}_i direction vectors and the global z -axis when the device is in its ‘home’ position (i.e. when the plane created by A_i joint positions is parallel to that defined by the B_i points). The value of β used here is 54.75° . Fourth, scalar constant γ indicates the angle between the \mathbf{u}_i direction vectors and the vertical axis (i.e. the global z -axis). Unlike β , this value is constant for all mechanism states because the joints corresponding to the \mathbf{u}_i direction vectors are fixed relative to the global frame. The value of γ used in this analysis is also 54.75° .

Finally, scalar constants η_1 , η_2 , and η_3 are used to specify the locations of the active joints associated with direction vectors \mathbf{u}_1 , \mathbf{u}_2 , and \mathbf{u}_3 and ‘home-positioned’ distal passive joints associated with \mathbf{v}_1 , \mathbf{v}_2 , and \mathbf{v}_3 within the global x - y plane. Measured with respect to the positive y -axis, the values of η_1 , η_2 , and η_3 are 0° , 120° , and 240° , respectively. Using this convention, η_i directly specifies the directions \mathbf{u}_i in the global x - y plane and specifies the directions \mathbf{v}_i in the global x - y plane when added to 60° and the mechanism is in its ‘home’ position. Note that the above parameter values are not independent, as they are related through geometry.

Equations for the \mathbf{u}_i direction vectors can be derived in terms of the η_i and γ parameters discussed above. This derivation involves the following fixed-frame rotation process: rotation of a local frame F_1 (i.e. originally identical to the global frame) by $(90^\circ - \eta)$ about the global 0y -axis and then rotation of F_1 by η_i about the 0z -axis. This overall transformation is represented mathematically in Kucuk and Bingul.¹⁷ Note that a superscript ‘0’ indicates an axis or vector expressed with respect to the global frame.

$$R_{01} = R_z(\eta_i + 90^\circ)R_y(90^\circ - \gamma) = \begin{bmatrix} -S\eta_i S\gamma & -C\eta_i & -S\eta_i C\gamma \\ C\eta_i S\gamma & -S\eta_i & C\eta_i C\gamma \\ -C\gamma & 0 & S\gamma \end{bmatrix} \quad (1)$$

It follows that the x -axis of the resulting R_{01} orientation frame is equal to the direction vector \mathbf{u}_i .

$$\mathbf{u}_i = \begin{bmatrix} -S\eta_i S\gamma \\ C\eta_i S\gamma \\ -C\gamma \end{bmatrix}^T \quad (2)$$

Direction vectors \mathbf{w}_i are in turn related to the corresponding \mathbf{u}_i vectors through a fixed rotation by α_1 within the plane containing O , A_i , and C_i , along with a variable rotation dependent on actuator angle θ_i .

The parameterization of this transformation can be considered as a set of current frame rotations: first a rotation of θ_i about the local x -axis and then a rotation of α_1 about the updated local z -axis. In matrix format, an expression for this is as follows.

$$R_x(\theta_i)R_z(\alpha_1) = \begin{bmatrix} C\alpha_1 & -S\alpha_1 & 0 \\ -S\theta_i S\alpha_1 & -S\theta_i C\alpha_1 & -C\theta_i \\ C\theta_i S\alpha_1 & C\theta_i C\alpha_1 & -S\theta_i \end{bmatrix} \quad (3)$$

Now, to obtain expression in terms of the global coordinate system, the set of rotations described above must be pre-multiplied by R_{01} . Finally, the set of direction vectors \mathbf{w}_i is obtained from the resulting matrix set as the x -axes for each i , as shown below.

$$\mathbf{w}_i = \begin{bmatrix} (-S\eta_i C\gamma C\theta_i + C\eta_i S\theta_i)S\alpha_1 - S\eta_i S\gamma C\alpha_1 \\ (C\eta_i C\gamma C\theta_i + S\eta_i S\theta_i)S\alpha_1 + C\eta_i S\gamma C\alpha_1 \\ -C\gamma C\alpha_1 + S\gamma C\theta_i S\alpha_1 \end{bmatrix}^T \quad (4)$$

Similarly to the derivation for \mathbf{u}_i vectors summarized in equations (1) and (2), the \mathbf{v}_i vectors can be established via two spatial rotations as follows when the device is in its 'home' position.

$$R_{03} = R_z(\eta_i)R_y(\beta) \quad (5)$$

Again, \mathbf{v}_i is given as the x -axis component of the orientation matrix shown in equation (5). To determine the \mathbf{v}_i directions after the mechanism's end-effector has undergone roll, pitch, and/or yaw rotations, R_{03} must be pre-multiplied by another transformation.

$$R_{04} = R_{rpy}R_{03} \quad (6)$$

where R_{rpy} represents the orientation of the end-effector with respect to the global frame. If it is assumed that R_{rpy} is expressed as fixed-frame rotations about the global x -axis by θ , y -axis by ϕ , and z -axis by ψ , respectively, then the \mathbf{v}_i vector can be explicitly derived as follows.

$$\begin{bmatrix} v_{ix} \\ v_{iy} \\ v_{iz} \end{bmatrix} = \begin{bmatrix} 1 \\ 0 \\ 0 \end{bmatrix} \cdot R_z(\psi)R_y(\phi)R_x(\theta)R_{03} \quad (7)$$

Given that all direction vectors \mathbf{w}_i and \mathbf{v}_i are of unit length, the angle between corresponding \mathbf{w}_i and \mathbf{v}_i vectors is α_2 (by the parameter's definition), and the geometric definition of the vector dot product, the following equation relates the two sets of direction vectors.

$$\mathbf{w}_i \cdot \mathbf{v}_i = \cos\alpha_2 \quad i = 1, 2, 3 \quad (8)$$

Now, through substitution of equations (4) and (7) into equation (8), a set of relationships between the system inputs and outputs is obtained. Upon performing this substitution and simplifying the result, the following equation is produced.

$$A \times \tan^2(\theta_i/2) + B \times \tan(\theta_i/2) + C = 0 \quad i = 1, 2, 3 \quad (9)$$

where

$$A = (-C\eta_i C\gamma S\alpha_1 + C\eta_i S\gamma C\alpha_1)v_{iy} + \dots (S\eta_i C\gamma S\alpha_1 - S\eta_i S\gamma C\alpha_1)v_{ix} + \dots (-C\gamma C\alpha_1 - S\alpha_1 S\gamma)v_{iz} - c\alpha_2 \quad (10)$$

$$B = 2S\eta_i S\alpha_1 v_{iy} + 2C\eta_i S\alpha_1 v_{ix} \quad (11)$$

$$C = (-S\eta_i C\gamma S\alpha_1 - S\eta_i S\gamma C\alpha_1)v_{ix} + (-C\gamma C\alpha_1 + S\alpha_1 S\gamma)v_{iz} + (C\eta_i C\gamma S\alpha_1 + C\eta_i S\gamma C\alpha_1)v_{iy} - c\alpha_2 \quad (12)$$

It follows that the input angle required to achieve a desired end-effector positional output can be found with the following equation.

$$\theta_i = 2 \operatorname{atan2} \left(\frac{-B \pm \sqrt{B^2 - 4AC}}{2A} \right) \quad i = 1, 2, 3 \quad (13)$$

Equations (10)–(13) represent the solution to the inverse kinematics problem for the 3-RRR manipulator because they provide the required active joint states, θ_i , necessary to achieve a desired orientation of the end-effector. That is, once end-effector rotations θ , ϕ , and ψ are established, the associated angular states of the active revolute joints can be identified.

Jacobian analysis

A number of generally accepted performance indices for parallel manipulators are often published as a method for comparing various robotic manipulators.¹⁶ The values of these indices usually have physical significance and applications for design optimization.¹⁷ The three indices considered in this paper, which are manipulability, dexterity, and rotational sensitivity, all derive from the Jacobian matrix of a manipulator. Thus, the 3-RRR device's Jacobian development is discussed in this section, before the performance indices are examined in the next section.

To start, a vector \mathbf{q} is assigned to represent active joint variables while \mathbf{x} is used to characterize the end-effector's position. The kinematic constraints associated

with the device's limbs can be expressed as follows.

$$f(\mathbf{x}, \mathbf{q}) = \mathbf{0} \quad (14)$$

where f is an n -dimensional implicit function of \mathbf{q} and \mathbf{x} , and n is the active joint count within the mechanism. Now, time-differentiating equation (14) yields the following relationship between input joint rates and end-effector velocity.

$$\frac{\partial f}{\partial \mathbf{x}} \dot{\mathbf{X}} + \frac{\partial f}{\partial \mathbf{q}} \dot{\mathbf{q}} = \mathbf{0} \rightarrow \mathbf{J}_x \dot{\mathbf{X}} = \mathbf{J}_q \dot{\mathbf{q}} \quad (15)$$

As shown above, two components of the Jacobian are produced: \mathbf{J}_x and \mathbf{J}_q . The combination of these components yields the complete Jacobian matrix.

$$\dot{\mathbf{q}} = \mathbf{J}_q^{-1} \mathbf{J}_x \dot{\mathbf{X}} = \mathbf{J} \dot{\mathbf{X}} \quad (16)$$

It is important to note that the Jacobian associated with a parallel manipulator, as in equation (16), is derived as the inverse of a serial manipulator's Jacobian.¹⁵

when equation (15) is written once for each of $i = 1, 2,$ and 3 , three scalar equations are produced. These can be arranged in matrix form as follows.

$$\begin{bmatrix} (\mathbf{w}_1 \times \mathbf{v}_1)^T \\ (\mathbf{w}_2 \times \mathbf{v}_2)^T \\ (\mathbf{w}_3 \times \mathbf{v}_3)^T \end{bmatrix} \omega_b = - \begin{bmatrix} \mathbf{w}_1 \times \mathbf{u}_1 \cdot \mathbf{v}_1 & 0 & 0 \\ 0 & \mathbf{w}_2 \times \mathbf{u}_2 \cdot \mathbf{v}_2 & 0 \\ 0 & 0 & \mathbf{w}_3 \times \mathbf{u}_3 \cdot \mathbf{v}_3 \end{bmatrix} \dot{\mathbf{q}} \quad (17)$$

Combining equations (16) and (17) yields a complete form of the 3-RRR manipulator's Jacobian matrix.

$$\mathbf{J} = \mathbf{J}_q^{-1} \mathbf{J}_x = - \begin{bmatrix} \mathbf{w}_1 \times \mathbf{u}_1 \cdot \mathbf{v}_1 & 0 & 0 \\ 0 & \mathbf{w}_2 \times \mathbf{u}_2 \cdot \mathbf{v}_2 & 0 \\ 0 & 0 & \mathbf{w}_3 \times \mathbf{u}_3 \cdot \mathbf{v}_3 \end{bmatrix}^{-1} \times \begin{bmatrix} (\mathbf{w}_1 \times \mathbf{v}_1)^T \\ (\mathbf{w}_2 \times \mathbf{v}_2)^T \\ (\mathbf{w}_3 \times \mathbf{v}_3)^T \end{bmatrix} \quad (18)$$

Recall that vectors \mathbf{u}_i , \mathbf{w}_i , and \mathbf{v}_i can be computed from equations (2), (4), and (7), respectively.

Hip exoskeleton design based on performance indices

With the 3-RRR manipulator's Jacobian matrix derived, it is now possible to evaluate several of the device's performance indices. In doing so, two methods for attaching the device to the human body are considered, as shown in Figure 4. Furthermore, only flexion-extension and abduction-adduction motions are considered; the final major DOF of the hip joint (i.e. internal/external rotation) is assumed to be constant and oriented such that the knee's axis of rotation is perpendicular to the sagittal plane of the body. As can be deduced from Figure 3, the device's ψ angle corresponds to flexion/extension motions for Attachment Method 1, while ϕ is associated with those motions in Attachment Method 2; for both cases, θ corresponds to abduction/adduction motions. Additionally, a workspace range of $[-0.2 \ 0.2]$ radians for both flexion-extension and abduction-adduction motions was considered for all local performance studies. Finally, the results below are only applicable when the parameter values (i.e. for $\alpha_1, \alpha_2, \beta, \gamma, \eta_1, \eta_2,$ and η_3) are selected as per the discussion in Kinematic architecture section.

Manipulability

Forces experienced by joints within parallel manipulators tend to become large when such a device nears singular configurations.¹⁶ Thus, the ability to quantify a manipulator's nearness to singular configurations is useful. Manipulability is a common performance index used to accomplish this quantification. It is defined as the absolute value of the Jacobian's determinant,¹⁸ as given in equation (19). Alternatively, this index can be interpreted as the Jacobian matrix's minimum-magnitude eigenvalue.

$$\mu = \sqrt{|J^T J|} \quad (19)$$

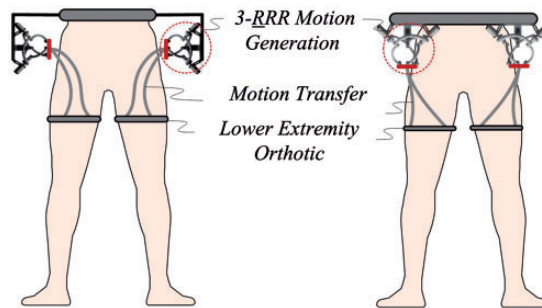


Figure 4. Considered 3-RRR attachment methods as a hip exoskeleton. (a) Interfacing scheme 1; (b) interfacing scheme 2.

In mechanical terms, manipulability represents a manipulator's ability to successfully create a desired velocity at its end-effector.¹⁹ Alternatively, this index can be understood as the ellipsoid volume resulting when a unit sphere is mapped from the manipulator's n -dimensional joint space into Cartesian space through its Jacobian matrix and a constant proportionality factor;²⁰ recall that n represents the active joint count for the manipulator. It follows that a manipulator achieves greater manipulability performance if its ellipsoid has a greater uniformity, or isotropy, characteristic.²¹ Such an isotropy index for manipulability can be quantified as follows.

$$\mu_{iso} = \sigma_{\min}/\sigma_{\max} \quad (20)$$

where σ_{\min} and σ_{\max} are the minimum and maximum singular values of the Jacobian matrix, respectively. The μ_{iso} value in equation (20) is limited to the range $[0, 1]$, where 0 indicates inability to transmit velocity to the end-effector (i.e. a singular configuration) and 1 indicates ability to transmit velocity to the end-effector uniformly in all directions. Figure 5 shows the 3-RRR device's manipulability deviation and statistical distribution within the considered workspace for the two attachment methods depicted in Figure 4.

According to the surface plots, the manipulability of the 3-RRR is greatest when operating near its 'home' configuration and least near the boundaries of the considered workspace for both attachment methods. Comparatively, Attachment Method 1 achieves a greater average value for manipulability than Attachment Method 2. Furthermore, Method 1 achieves less variance in performance within the workspace considered.

Therefore, Method 1 is superior to Method 2 in terms of manipulability.

Dexterity (condition number)

Because a manipulator's control scheme generally relies on its joint position coordinates, any errors between the expected and actual joint coordinates cause errors in the end-effector's position and orientation.¹⁶ This end-effector error can be determined through multiplication of the errors in the joint coordinates by a scaling factor: the condition number, k .²² A manipulator's condition number is obtained from the Jacobian matrix as follows.²²⁻²⁵

$$k(\mathbf{J}) = \|\mathbf{J}\| \|\mathbf{J}^{-1}\| \quad (21)$$

where \mathbf{J} is the Jacobian matrix. Here, $\|\mathbf{J}\|$ denotes the Jacobian's Euclidean norm.

$$\|\mathbf{J}\| = \sqrt{\text{tr}\left(\frac{1}{n}\mathbf{J}\mathbf{J}^T\right)} \quad (22)$$

Gosselin proposes that the condition number's inverse be used to quantify a manipulator's kinematic accuracy;²⁴ this criterion is called the local dexterity index, denoted by ν .

$$\nu = \frac{1}{\|\mathbf{J}\| \|\mathbf{J}^{-1}\|} \quad (23)$$

Again, allowable values for ν are constrained between 0 and 1; zero indicates a singularity, and

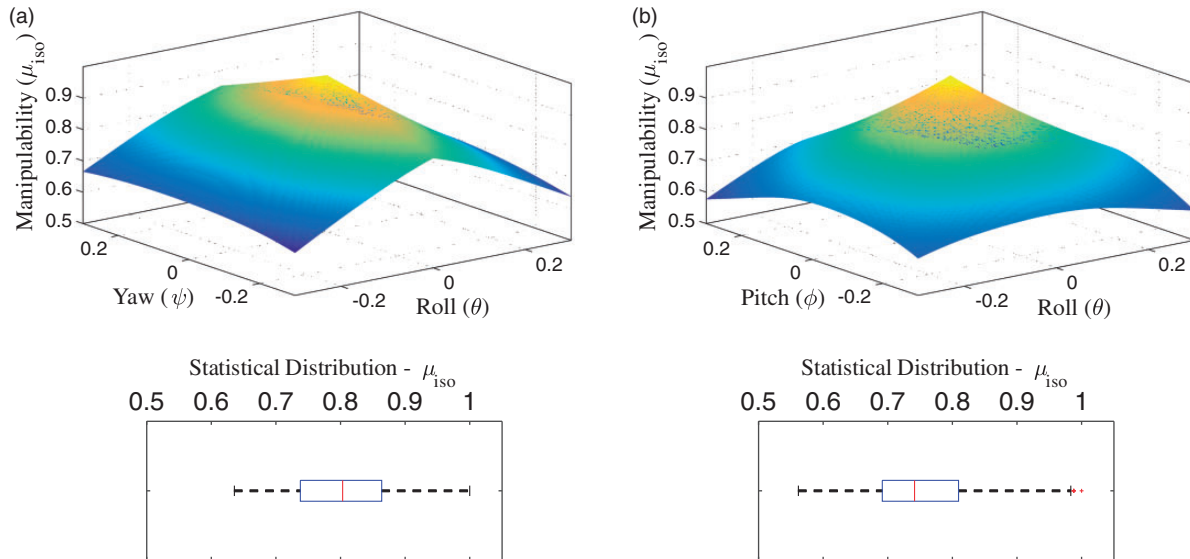


Figure 5. 3-RRR manipulability for (a) Attachment Method 1 and (b) Attachment Method 2.

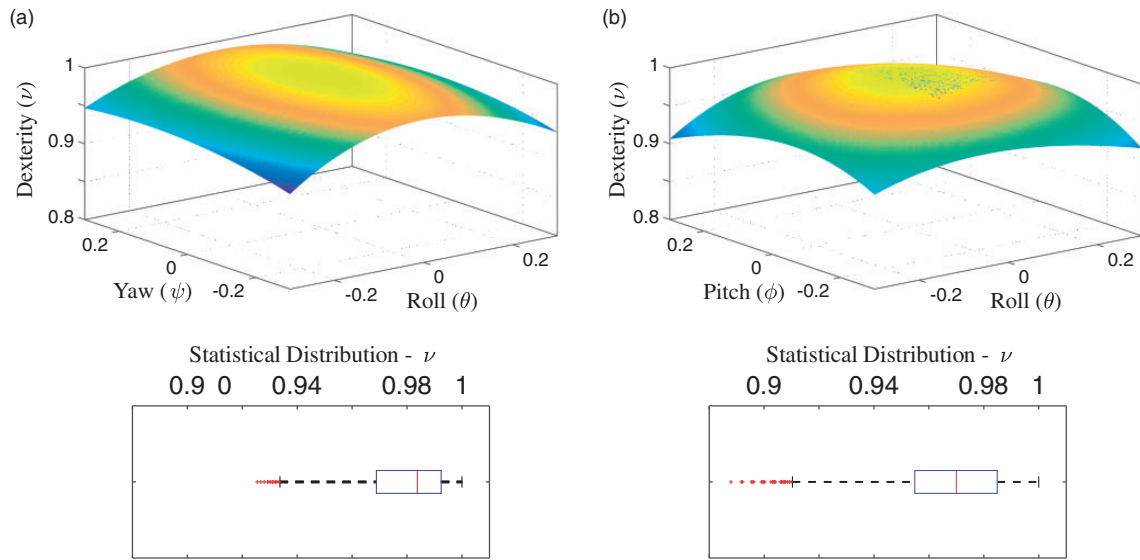


Figure 6. 3-RRR dexterity for (a) Attachment Method 1 and (b) Attachment Method 2.

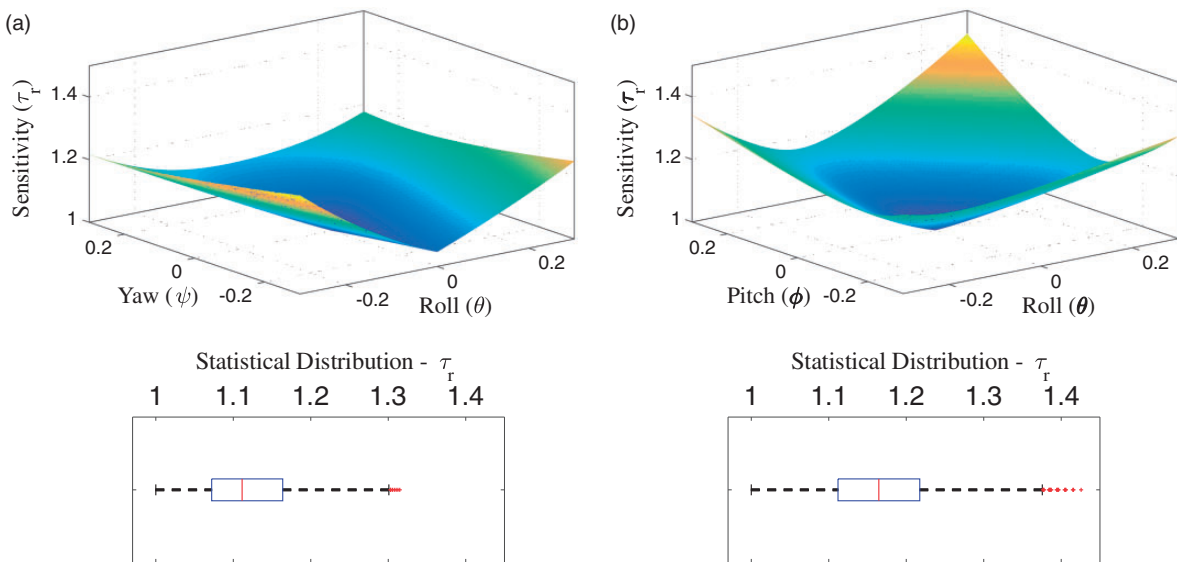


Figure 7. 3-RRR rotational sensitivity for (a) Attachment Method 1 and (b) Attachment Method 2.

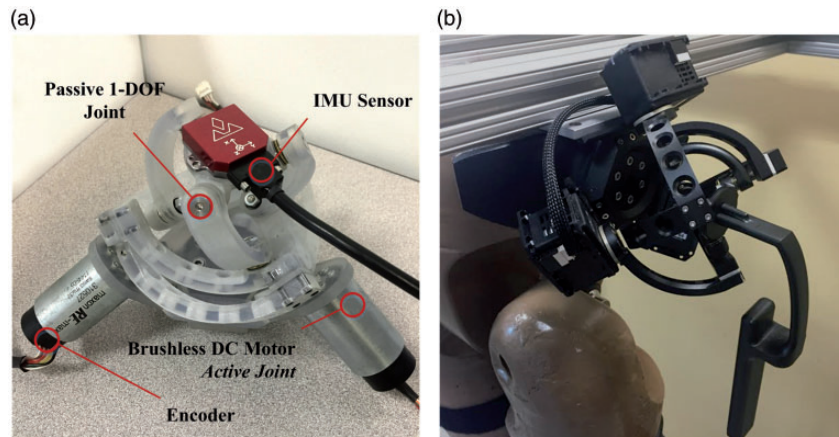


Figure 8. (a) Experimental prototype of the 3-RRR manipulator and (b) 3-RRR manipulator mounted on the Hip mannequin.

greater values correspond to increasingly accurate motion generation at the end-effector.

Figure 6 depicts dexterity index surface plots and statistical box plots for both body-attachment arrangements of the 3-RRR manipulator across its considered workspace. Similarly to manipulability, these plots suggest that the mechanism's dexterity is greatest when configured in close proximity to its 'home' orientation and that it decreases as the device moves towards the boundaries of its considered workspace. Additionally, greater average dexterity and less dexterity variation are achieved when the 3-RRR robot is interfaced with the human body according to Attachment Method 1 as opposed to Method 2, which makes the former preferable.

Rotational sensitivity

The rotational sensitivity index of a manipulator indicates how reactive its end-effector is to changes in active joint states. More specifically, it is the maximum-magnitude rotation of the end-effector under a unit-norm actuator displacement;²⁰ it is given by either the 2-norm or the ∞ -norm of the Jacobian matrix as follows.

$$\tau_r = \|J\| \quad (24)$$

Figure 7 shows the sensitivity results for the 3-RRR manipulator when subject to the body-interfacing schemes of Figure 4 and constrained to the $[-0.2, 0.2]$ radian workspace range in both flexion-extension and abduction-adduction motions. Again, Attachment Method 1 demonstrates preferable performance to that of Method 2 because the former possesses the smaller-magnitude average and variance range in sensitivity index value. Furthermore, sensitivity performance is optimal for both arrangements near the device's 'home' orientation and degrades as the workspace limits are approached.

Experimental study on the 3-RRR manipulator

Mechanism fabrication details

In preparation for experimental tests on the 3-RRR manipulator design proposed in this paper, a prototype system was fabricated. As shown in Figure 8, all linkage components of the device are 3D-printed, including the base structure, proximal and distal links, and end-effector platform. The prototype's passive revolute joints are composed of off-the-shelf shoulder screws, rotary ball bearings, and thrust bearings. Meanwhile, the active revolute joints are prototyped with Maxon RE-max 29 brushed DC motors. Lastly, a VectorNAV

VN-100 Rugged inertial measurement unit (IMU) is attached to the end-effector platform for capturing orientation data during system operation.

Experimental results

The purpose of our experimental study on the 3-RRR prototype is to confirm its end-effector's ability to perform the 3-DOF motions experienced by the human hip joint during normal gait cycles. In order to complete this test, the prototype's motors are controlled with a simple proportional-integral (PI) scheme; angular feedback is provided by the actuator's attached encoders.

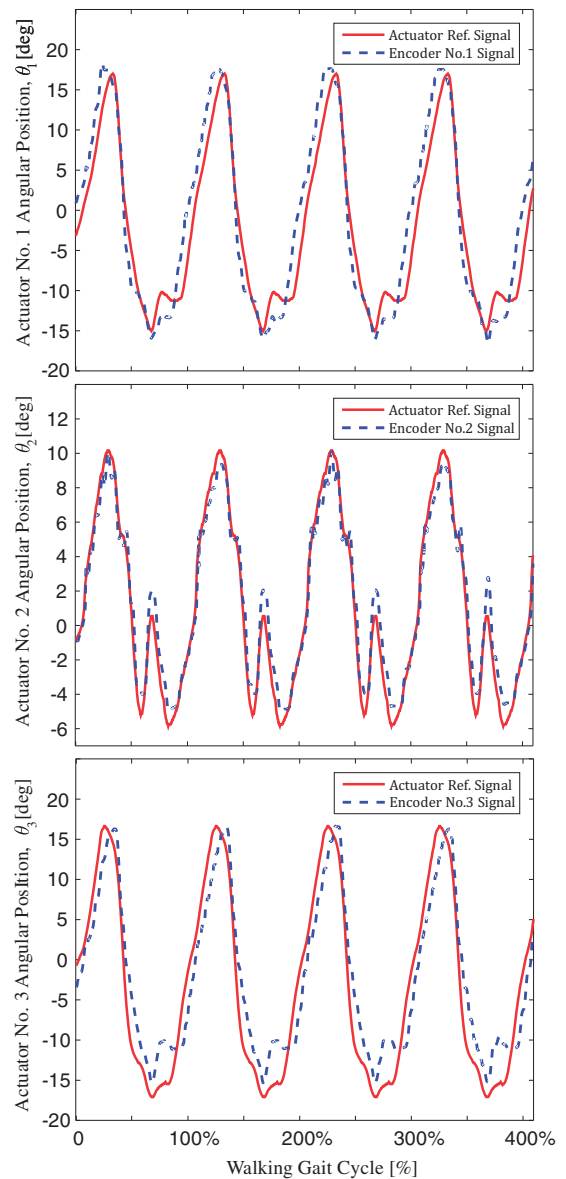


Figure 9. Comparison of reference signal and encoder feedback from each actuator during gait motion tracking.

In terms of test execution, reference signals for the end-effector to track are provided by Stanford University's OpenSim software.^{26,27} Subsequently, motor reference signals are obtained by applying the inverse kinematics algorithm discussed in Kinematic architecture section to the OpenSim angular motion signals. Because Attachment Method 1 is expected to provide manipulability, dexterity, and sensitivity performance that are superior to those of Method 2, the motion strategy associated with Method 1 is utilized. That is, the

prototype's ψ motions are matched to hip flexion-extension motions, θ to abduction-adduction, and ϕ to internal/external rotations.

The experimental results of Figure 9 depict the reference and response signals associated with the individual system motors. These are the motions required by the selected design and body-attachment scheme to achieve the hip motions associated with normal gait cycles at the end-effector, as determined by the inverse kinematics algorithm. In turn, Figure 10 presents an

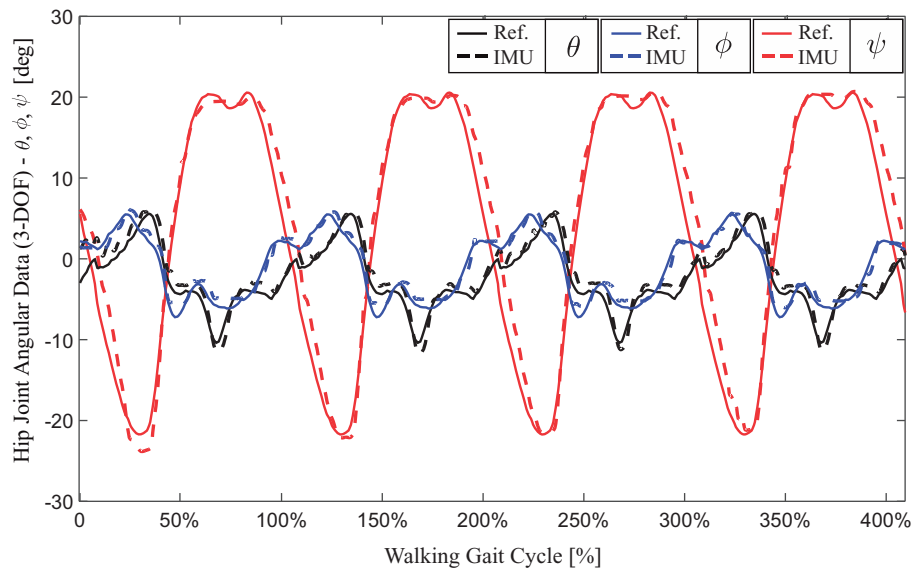


Figure 10. Comparison of desired end-effector orientation and IMU-measured value during gait motion tracking.

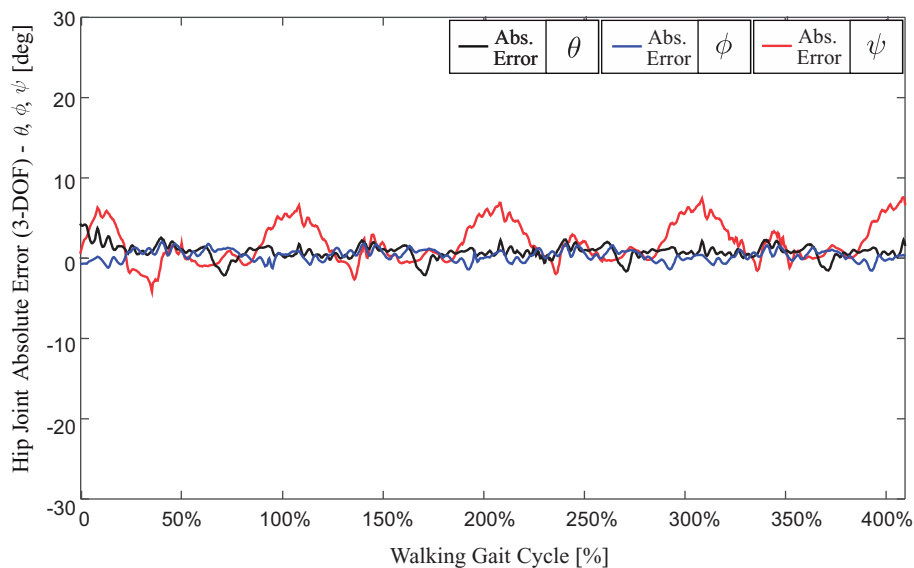


Figure 11. Absolute error between desired end-effector orientation and IMU-measured value during gait motion tracking.

overlay of the resulting end-effector orientation angles, as captured by the system IMU, and the desired angles, as provided by the OpenSim software.

The results shown in Figures 9 and 10 indicate that the 3-RRR manipulator can achieve the same motion ranges as the human hip during normal gait cycles. Furthermore, the plots suggest that the mechanism can complete these motions with a similar rate to that of the human hip. The maximum absolute error between a single desired end-effector angle and the measured angle is 7.6° , and it applies to ψ (i.e. flexion-extension motions); the root mean squared error values for θ , ϕ , and ψ are 1.2° , 0.7° , and 3.1° , respectively.

As shown in the absolute error plots of Figure 11, the error in ψ rises periodically during a rapid extension motion of the hip joint. This systematic error can be primarily attributed to the experiment's non-optimal control method, which does not account for inherent nonlinearities of the device's dynamics and inhibits the device from adequately tracking its reference signal. Therefore, the development of a more effective control algorithm would likely reduce the end-effector's orientation errors. Given this solution and the otherwise small magnitudes of error, it is feasible that the 3-RRR manipulator could be used within a hip exoskeleton system.

Conclusion and future work

This paper proposes the use of the well-established 3-RRR manipulator as a robotic component within a hip exoskeleton system. Before investigating the mechanism's performance for two different body-attachment methods and presenting the results of a motion-tracking experiment, the device's inverse kinematics and Jacobian matrix development procedures were revisited.

The performance study results indicate that the body-interfacing arrangement that orients the manipulator's x - y plane parallel to the body's sagittal plane is superior in terms of average value and variability for manipulability, dexterity, and rotational sensitivity indices. As can be expected, the manipulator's performance is optimal when configured at its initial 'home' orientation and degrades as the end-effector moves away from this state.

For the experimental study, a prototype manipulator's end-effector was controlled to track the motions experienced by a human hip joint during normal gait cycles. In summary, the general agreement between input and output signals depicted in the resulting figures suggests that application of this 3-RRR design as a hip exoskeleton is feasible. Furthermore, this application poses a motion assistance solution with total kinematic compliance for multi-DOF body joints. Future work includes singularity, dynamic, and workspace

analyses, design and analysis of the complete exoskeleton system with bodily interfacing details considered, and development of an effective closed-loop control algorithm for the 3-RRR manipulator.

Declaration of Conflicting Interests

The author(s) declared no potential conflicts of interest with respect to the research, authorship, and/or publication of this article.

Funding

The author(s) disclosed receipt of the following financial support for the research, authorship, and/or publication of this article: This work was supported by the Natural Sciences and Engineering Research Council of Canada (NSERC).

References

1. W. Erickson, C. Lee and S. von Schrader. *Disability statistics from the 2013 American Community Survey (ACS)*. Ithaca, NY: Cornell university, 2015.
2. Statistics Canada. *Disability in Canada: Initial findings from the Canadian Survey on Disability*. Ottawa: Canadian Survey on disability.
3. Li Z, Xie H, Li W, et al. Proceeding of human exoskeleton technology and discussions on future research. *Chin J Mech Eng* 2014; 27: 437–447.
4. Cenciarini M and Dollar AM. Biomechanical considerations in the design of lower limb exoskeletons. *IEEE Int Conf Rehabil Robot* 2011; 2011: 1–6.
5. Esquenazi A, Talaty M, Packel A, et al. The ReWalk powered exoskeleton to restore ambulatory function to individuals with thoracic-level motor-complete spinal cord injury. *Am J Phys Med Rehabil* 2012; 91: 911–921.
6. Ambrose RO, Aldridge H, Askew RS, et al. Robonaut: NASA's space humanoid. *IEEE Intell Syst Appl* 2000; 15: 57–63.
7. Kizir S and Bingul Z. Position control and trajectory tracking of the Stewart platform. In: Kucuk S (ed.) *Serial and parallel robot manipulators - kinematics, dynamics, control and optimization*. Istanbul, Turkey: InTech, Chapters published under CC BY 3.0 license, 2012, 179–202.
8. Gosselin C and Angeles J. The optimum kinematic design of a spherical three-degree-of-freedom parallel manipulator. *J Mech Transm Autom Des* 1989; 111: 202–207.
9. Gosselin CM and Lavoie E. On the kinematic design of spherical three-degree-of-freedom parallel manipulators. *Int J Rob Res* 1993; 12: 394–402.
10. Gosselin CM and Hamel J-F. The agile eye: A high-performance three-degree-of-freedom camera-orienting device. In: *Proceedings of the 1994 IEEE International Conference on Robotics and Automation*, San Diego, pp.781–786.
11. Gosselin CM and St-Pierre E. Development and experimentation of a fast 3-DOF camera-orienting device. *Int J Robot Res* 1997; 16: 619–630.

12. Bai S, Hansen MR and Angeles J. A robust forward-displacement analysis of spherical parallel robots. *Mech Mach Theory* 2009; 44: 2204–2216.
13. Wang C, Fang Y, Guo S, et al. Design and kinematical performance analysis of a 3-RUS/RRR redundantly actuated parallel mechanism for ankle rehabilitation. *J Mechanisms Robotics* 2013; 5: 1–11.
14. Niyetkaliyev A and Shintemirov A. An approach for obtaining unique kinematic solutions of a spherical parallel manipulator. In: *2014 IEEE/ASME International Conference on Advanced Intelligent Mechatronics*, Besançon, France, 2014, 1355–1360.
15. Tsai L. *Robot analysis: The mechanics of serial and parallel manipulators*. New York, NY: J. Wiley and Sons, 1999.
16. Merlet J-P. *Parallel Robots*, 2nd ed. Sophia-Antipolis, France: Springer, 2006.
17. Kucuk S and Bingul Z. Comparative study of performance indices for fundamental robot manipulators. *Rob Auton Syst* 2006; 54: 567–573.
18. Yoshikawa T. Manipulability of robotic mechanisms. *Int J Robot Res* 1985; 4: 3–9.
19. Mansouri L and Ouali M. The power manipulability – A new homogeneous performance index of robot manipulators. *Robot Comput Integr Manuf* 2011; 27: 434–449.
20. Cardou P, Bouchard S and Gosselin C. Kinematic-sensitivity indices for dimensionally nonhomogeneous Jacobian matrices. *IEEE Trans Robot* 2010; 26: 166–173.
21. Angeles J and Lopez-Cajun CS. Kinematic isotropy and the conditioning index of serial robotic manipulators. *Int J Robot Res* 1992; 11: 560–571.
22. Stoughton RS and Arai T. Modified Stewart platform manipulator with improved dexterity. *IEEE Trans Robot Autom* 1993; 9: 166–172.
23. Pittens KH and Podhorodeski RP. A family of Stewart platforms with optimal dexterity. *J Robot Syst* 1993; 10: 463–479.
24. Rao ABK, Rao PVM and Saha SK. Workspace and dexterity analyses of hexaslide machine tools. In: *Proceedings of ICRA '03, IEEE International Conference on Robotics and Automation*, Vol. 3, Taipei, Taiwan, 2003, pp.4104–4109.
25. Gosselin CM. The optimum design of robotic manipulators using dexterity indices. *Rob Auton Syst* 1992; 9: 213–226.
26. Delp SL, Loan JP, Hoy MG, et al. An interactive graphics-based model of the lower extremity to study orthopaedic surgical procedures. *IEEE Trans Biomed Eng* 1990; 37: 757–767.
27. Anderson FC and Pandy MG. A dynamic optimization solution for vertical jumping in three dimensions. *Comput Methods Biomech Biomed Engin* 1999; 2: 201–231.